Nuclear Materials and Energy 41 (2024) 101812

Contents lists available at ScienceDirect

Nuclear Materials and Energy

journal homepage: www.elsevier.com/locate/nme

Study of spectral features and depth distributions of boron layers on tungsten substrates by ps-LIBS in a vacuum environment

Huace Wu [a,b], Rongxing Yi [b], Anne Houben [b], Sebastijan Brezinsek [b,*], Marcin Rasinski [b], Cong Li [a], Gennady Sergienko [b], Yunfeng Liang [b], Timo Dittmar [b], Hongbin Ding [a,*]

[a] *Key Laboratory of Materials Modification by Laser, Ion and Electron Beams (Ministry of Education), School of Physics, Dalian University of Technology, 116024 Dalian, PR China*

[b] *Forschungszentrum Jülich, Institute of Fusion Energy & Nuclear Waste Management – Plasma Physics, 52425 Jülich, Germany*

ARTICLE INFO

Keywords:
Boronization
Boron-films on the W-substrates
Depth ablation rate
Interface determination
Ps-LIBS

ABSTRACT

Boronization is used in present-devices as wall condition technique due to its effectiveness in reducing oxygen and other impurities in the vessel as well as improving plasma performance. The technique is also currently under consideration as wall conditioning method for the proposed full-tungsten (W) wall of the International Thermonuclear Experimental Reactor (ITER). However, the impact of the deposited Boron (B) layer thickness, and its homogeneity after the boronization process is uncertain as well as knowledge about the layer lifetime and improved conditions. In this study, an approach of the picosecond-laser-induced breakdown spectroscopy (ps-LIBS) is investigated to analyze the depth distribution of B-films on W-substrates by using three optical spectrometers in a vacuum environment. The depth distribution of two types of B-films on W-substrates with the thicknesses of 130 nm and 260 nm were sequentially measured under different laser spot sizes (varying the laser fluence). The B-films on the W-substrates were made by magnetron sputtering to simulate the thin B layers during the boronization. The measured average ablation rate of ps-LIBS shows a notable decrease with increasing laser spot size. Additionally, the spectral lines of B and W exhibit distinct intensity distributions under different spot sizes due to the different excitation thresholds of the B-films and the W-substrates. The interface between B-films and W-substrates, as well as the thickness of the B-films, were determined using the normalized intensity and intensity ratio method, respectively. The results from ps-LIBS measurements regarding the depth are in good agreement with those obtained through the Focused Ion Beam combined with Scanning Electron Microscopy (FIB-SEM) and Energy Dispersive X-ray Spectroscopy (EDS). These initial findings verify the feasibility to characterize the thickness and uniformity of thin B films in the order of 100 nm and below on W-substrates using ps-LIBS.

1. Introduction

Boronization is considered as routine wall conditioning technique to ease operation with the proposed full-tungsten (W) plasma-facing material option [1]. Boron (B) acts primarily as oxygen getter, but can also reduce intrinsic impurities content such as carbon and nitrogen as well as moderately reduced the hydrogen recycling by both gettering and surface layer coverage [2,3]. However, the B layers thickness induced by the boronization process and the subsequent lifetime is limited by plasma-induced erosion. Moreover, the B layers are not necessarily toroidal and poloidal homogeneous, and repetitively boronization needs to be applied to be effective if the gettering effect is lost [4]. The dynamic evolution of boron films in each region of the first wall after boronization needs to be investigated in real time and *in-situ*. This is essential for controlling the wall conditions and optimizing the wall treatment methods. Additionally, it will help to better understand the physical mechanisms of plasma-wall interactions (PWI) in metallic walls with boron in hydrogenic plasma [5,6]. Thus, a LIBS system using a laser installed in a (toroidal) device is the long-term goal for the described *in-situ* studies.

At present, boronization, typically a He glow-discharge cleaning (GDC) plasma with typically 5–10 % of diborane in it, has been successfully applied to many fusion devices. These include the TEXTOR and the stellarator Wendelstein 7-X (W7-X) with graphite walls, the Korea

---

* Corresponding authors.
E-mail addresses: s.brezinsek@fz-juelich.de (S. Brezinsek), hding@dlut.edu.cn (H. Ding).

https://doi.org/10.1016/j.nme.2024.101812
Received 6 August 2024; Received in revised form 31 October 2024; Accepted 9 November 2024

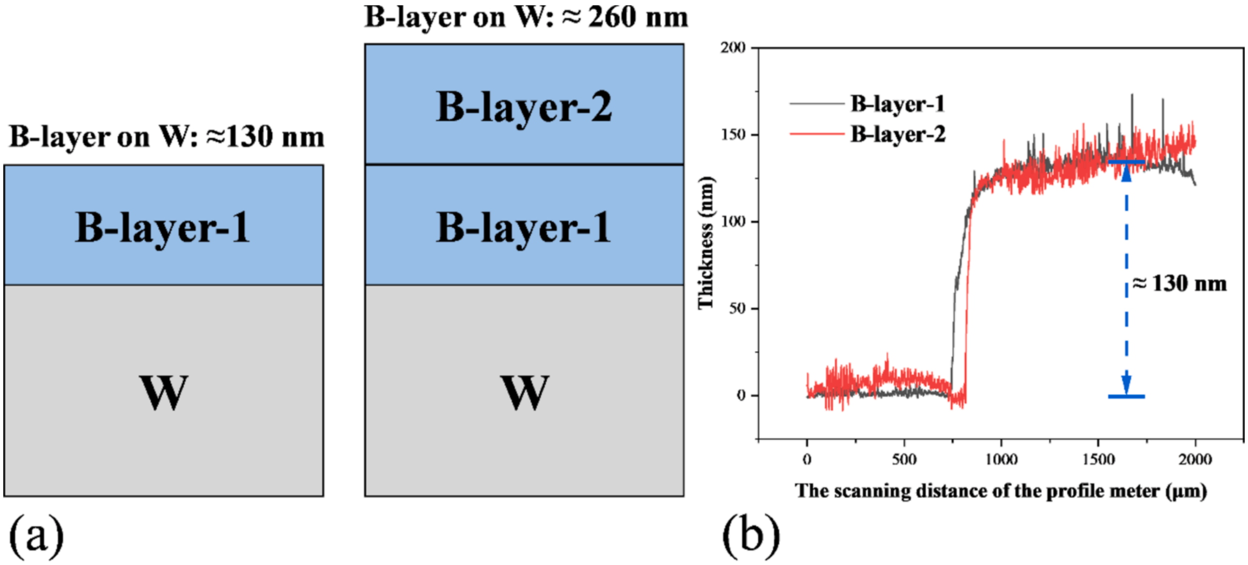

Fig. 1. (a) The boron (B) films with different thicknesses on pure tungsten (W) samples obtained by magnetron sputtering; (b) the thicknesses profile of B layers after the magnetron sputtering measured by profiler. The surface roughness (Ra) of the B-layer-1 and B-layer-2 is about 4.58 nm and 7.07 nm, respectively.

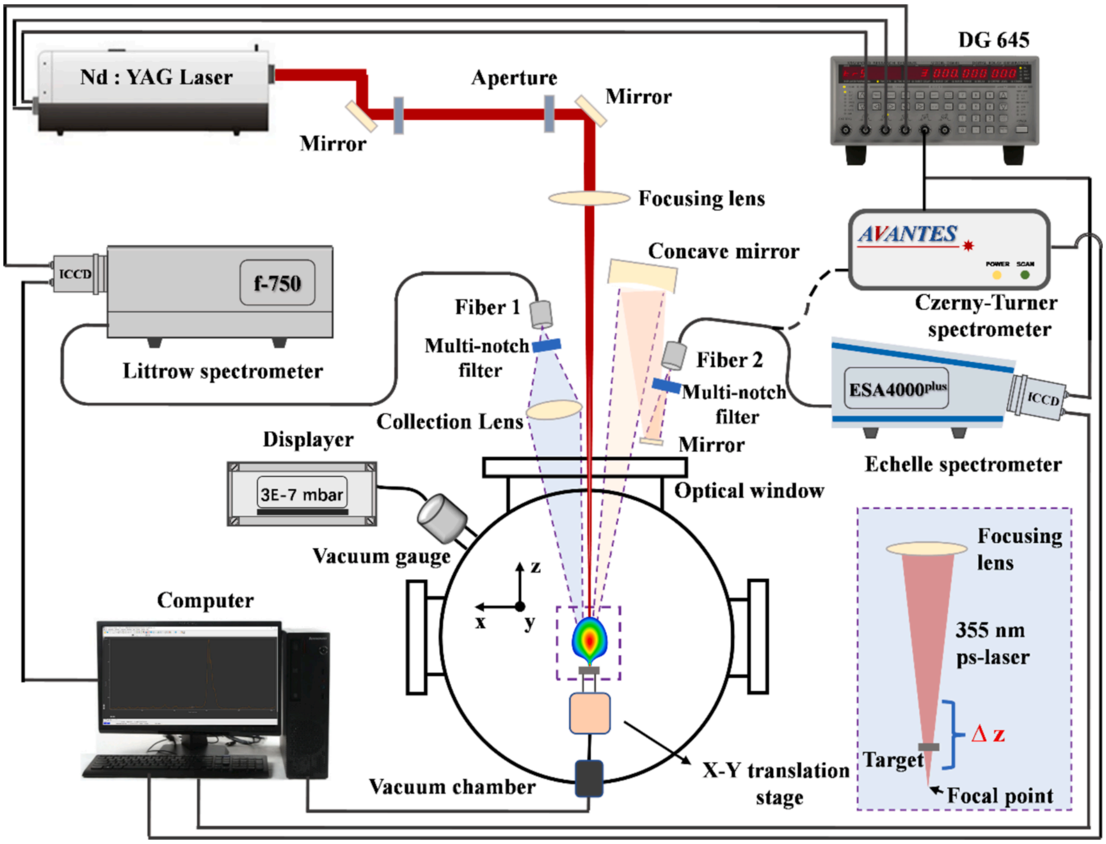

Fig. 2. Schematic diagram of the picosecond-LIBS experimental setup.

Superconducting Tokamak Advanced Research (KSTAR), ASDEX Upgrade (AUG), Experimental Advanced Superconducting Tokamak (EAST) and the W Environment in Steady-state Tokamak (WEST) with W walls. This technique has achieved good plasma operation results owing to the condition effects mentioned above [7–11]. On the one hand, before tokamak or stellarator plasma operation, the B_2H_6 and B_2D_6 gas is injected by helium or deuterium GDC to achieve the covering of B films on the plasma-facing surfaces and the gettering effect or $C_2B_{10}H_{12}$ and B_4C solid powders are heated and evaporated by crucible [7,12,13]. On the other hand, as the long pulse fusion devices like W7-X, EAST, KSTAR continuously push the limits of their operational space, the real-time wall conditioning technique such as impurity powder dropper (IPD) has been developed to maintain optimum wall conditions between plasma discharges [14,15]. To characterize the actual wall conditions and, thus the impact on the plasma performance, the real-time characterization of B-films on the first wall in or between tokamak discharge is

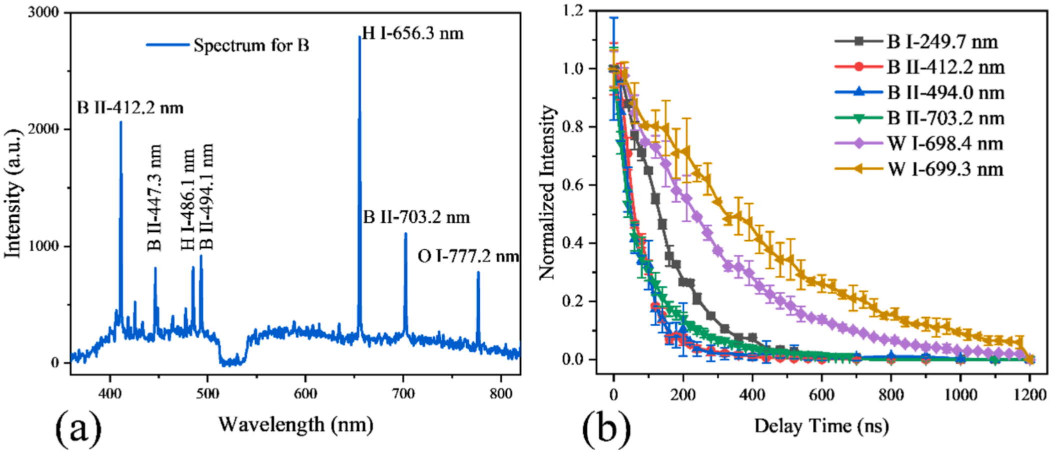

Fig. 3. (a) The typical B spectrum at the first laser pulse with spot size of 566 μm (7.2 J/cm^2) of the B-layer on W substrate; (b) Temporal evolution of spectral lines intensity of B and W. The zero time of delay time is set to coincide with the laser pulse peak.

Table 1
Laser spot sizes and corresponding laser fluence.

Spot size diameter (μm)	142	254	439	566	662	772	892	916
Laser fluence (J/cm^2)	113.6	35.5	11.8	7.2	5.2	3.9	2.9	2.7
Spot size diameter (μm)	980	1079	1137	1297	1375	1414	1518	
Laser fluence (J/cm^2)	2.4	2.0	1.8	1.4	1.2	1.1	1.0	

Table 2
Spectroscopic parameters of B and W characteristic lines [39].

	Wavelength (nm)	Energy of upper state, E_k (eV)	Energy of lower state, E_i (eV)	Transition Probability, A_{ki} (10^6 s^{-1})	Statistical weight, g_k
B I	249.68	4.96	0.00	84	2
B I	249.77	4.96	0.002	168	2
B II	412.19	21.69	18.68	236	9
B II	494.04	21.69	19.18	188	7
B II	703.02	17.85	16.09	39.7	5
B II	703.19	17.85	16.09	39.8	3
B II	703.25	17.85	16.09	39.7	1
W I	698.43	3.43	1.66	0.044	5
W I	699.33	4.23	2.46	0.058	9
H I	656.28	12.09	10.20	64.7	6
O I	777.19	10.74	9.15	36.9	7

of high values [16]. The boron films will lose its function due to the plasma induced erosion during long pulse operation. This requires an accurate judgment of the B-film features with various discharge times. Therefore, an approach for precisely measuring homogeneity and thickness of deposited B-coatings remains to be developed with *in-situ* and real-time techniques.

Laser-induced breakdown spectroscopy (LIBS) is a powerful approach for the analysis of the element composition [17,18]. Due to its unique advantages such as non-intrusive, no sample preparation requirement, large-area scanning, multi-elemental analytical ability, remote and in-situ capability, etc., LIBS technique is considered a potential candidate for *in-situ* investigations of erosion, deposition and material mixing in nuclear fusion devices [19–24]. In the past two decades, *in-situ* LIBS technology has achieved successful applications in TEXTOR, EAST, Joint European Torus (JET) and Frascati Tokamak Upgrade (FTU) as well as in linear plasma devices such as Magnum-PSI and PSI-2 [25–30]. As a 3-D analysis technology based on pulsed laser, LIBS can obtain the important information like homogeneity and thickness distribution B-layers. Gierse et al. first successfully obtained B signals using nanosecond (ns) LIBS technique on the W belt limiter of TEXTOR, which directly demonstrated the feasibility of using *in situ* LIBS to detect relevant B information on the wall surface [31]. Sun et al. analyzed the impurity features deposited on the W tiles exposed in KSTAR after wall boronization using ns LIBS in the laboratory [32]. Zhao et al. investigated the boron distribution on the W7-X divertor tiles by picosecond (ps) LIBS in the laboratory [33]. Their results all demonstrate the heterogeneity of B distribution on the divertor tiles surface after a round of campaign. However, the laser ablation properties of B films on W-substrate in fusion-like environment needs to be further studied systematically, which is of great significance for *in-situ* measurement analysis of the dynamic evolution of B on the wall surface. In ns-LIBS, the longer pulse width (compared to the typical electron-lattice relaxation time of $\sim 10^{-12}$ s) can lead to significant thermal diffusion inside the sample. For a 10 ns laser, commonly used in ns-LIBS, the thermal diffusion length in a tungsten (W) wall is on the order of one micrometer. This diffusion can create a large heat-affected zone, thereby limiting the resolution in both depth and lateral directions. Additionally, when the plasma density approaches the critical point, part of the ns laser pulse energy may be absorbed before reaching the target surface, resulting in a strong plasma shielding effect. This is considered a detrimental factor for achieving accurate LIBS measurements. Compared with ns-LIBS, ps-LIBS is supposed to be more suitable for the depth distribution analysis of the multilayer samples because it can reduce the heat-affected zone of the target, reduce the plasma shielding effect and so on [34,35].

In this work, as a first step, the typical B spectra and the temporal evolution of spectral intensity of B and W lines were characterized systematically in a vacuum set-up in the laboratory. Subsequently, according to the optimized spectral acquisition parameters, the depth distribution of two B films with different thicknesses on W-substrate were analyzed under the different laser spot sizes (laser fluence). The

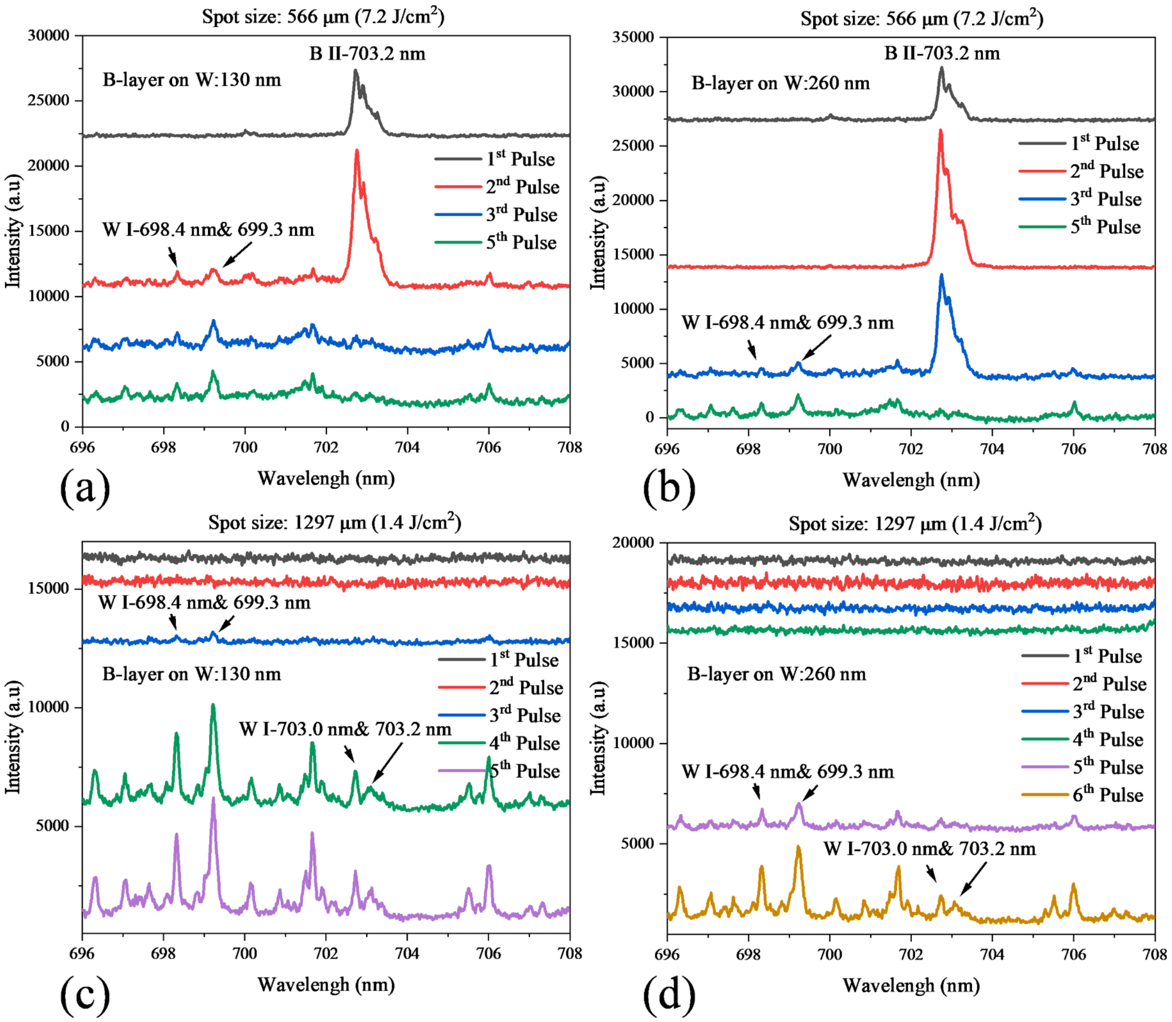

Fig. 4. The spectra of B layers about (a) 130 nm and (b) 260 nm at the spot size of 566 μm (7.2 J/cm^2) under different laser pulses; the spectra of B layers about (c) 130 nm and (d) 260 nm at the spot size of 1297 μm (1.4 J/cm^2) under different laser pulses. These spectra were acquired by Littrow spectrometer.

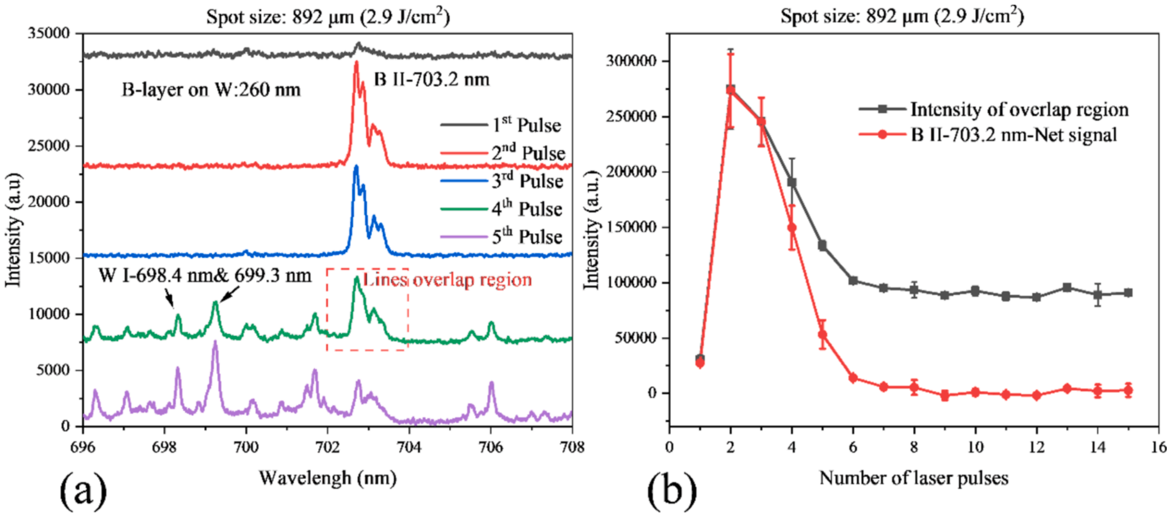

Fig. 5. (a)The variation of spectral intensity of B-layer sample for the first five pulses at the spot size of 892 μm (2.9 J/cm^2) and (b) depth distribution of B signal before and after correction.

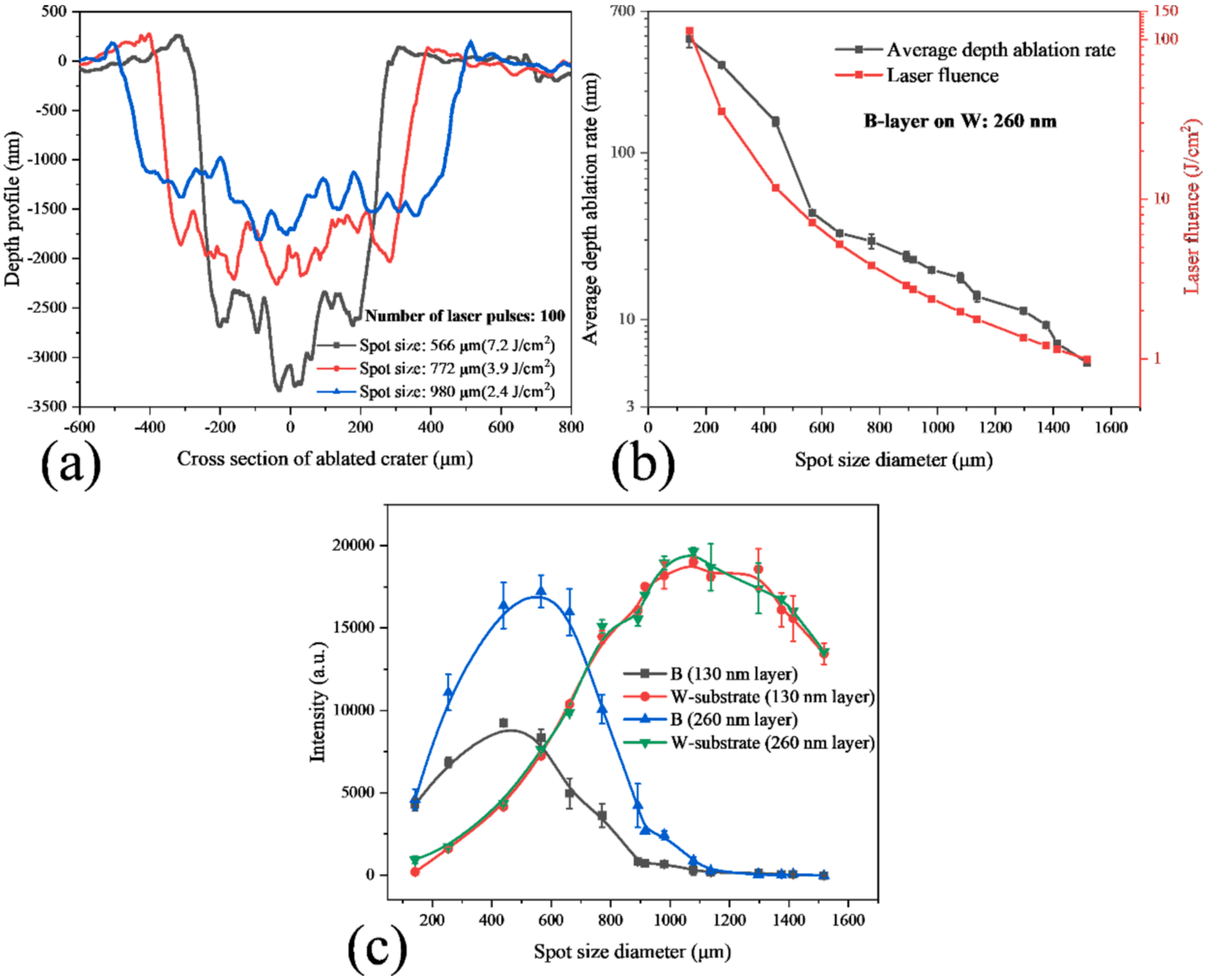

Fig. 6. (a) The depth profile of the B-layer (about 260 nm) on W sample after 100 laser pulses with spot size of 566 μm (7.2 J/cm^2),771 μm (3.9 J/cm^2), and 980 μm (2.4 J/cm^2), respectively. (b) The average depth ablation rate of the sample (260 nm B-layer on W) after 100 laser pulses and laser fluence corresponding to the different spot size diameters. (c) Comparison of B and W spectral line intensity with the spot size diameters under the two different B film thicknesses. The B signal intensity is the sum of the net B signal at first 10 laser pulses and the W signal intensity is the sum of the 11th to 20th pulses.

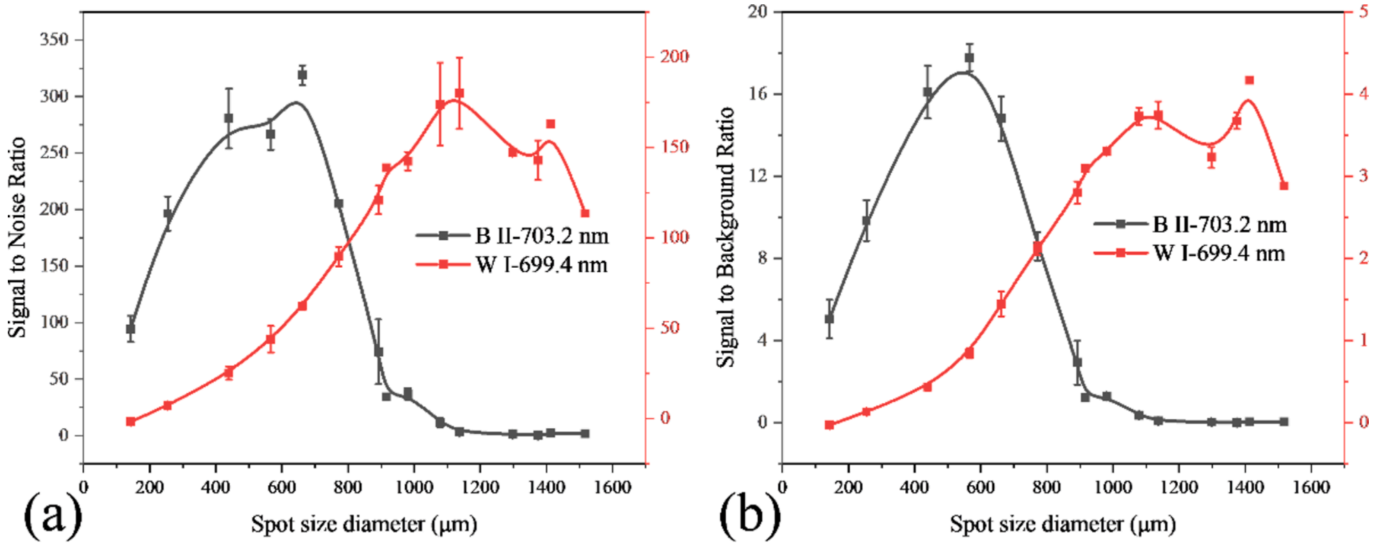

Fig. 7. The variation of (a) S/N and (b) S/B of of B II-703.2 nm and W I-699.4 nm with different spot size diameters.

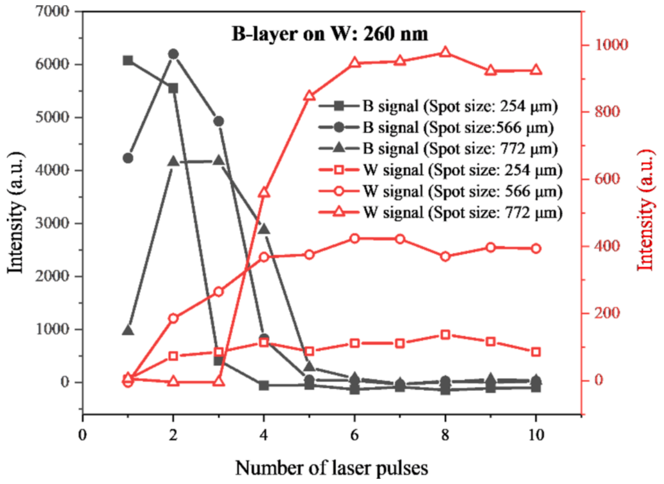

Fig. 8. Comparison of the depth distribution of B signal and W signal for the B-layer (about 260 nm) on W sample with different spot size diameters.

Table 3
The number of laser pulses required at the interface between B layer and W substrate and the average ablation rate of the B layer under different spot sizes calculated by normalized intensity method.

	B-layer on W: 130 nm		B-layer on W: 260 nm	
Spot size (μm)	Number of laser pulses	Average ablation rate (nm/pulse)	Number of laser pulses	Average ablation rate (nm/pulse)
254 (35.5 J/cm^2)	1.70 ± 0.078	75.63 ± 3.38	2.28 ± 0.046	121.64 ± 2.42
566 (7.2 J/cm^2)	2.21 ± 0.007	57.91 ± 0.17	3.23 ± 0.081	85.75 ± 2.15
772 (3.9 J/cm^2)	3.18 ± 0.118	40.38 ± 1.52	4.14 ± 0.018	66.98 ± 0.29

spectral signal quality and depth resolution of B layers on W-substrate under the different spot sizes were further investigated. Finally, the improving measurements for the thickness of B layers on W-substrate using the optimal parameters were determined.

2. Experimental setup and sample preparation

2.1. Sample preparation and characterization

A set of grinded and polished W targets (10 mm × 10 mm × 5 mm, double-forged W with 99.99 % purity, produced by Plansee SE according to the ITER specifications) were used as the substrate sample. Subsequently, the W substrate samples were outgassed and stress-relieved at 1273 K for 1 h in a vacuum before B deposition via magnetron sputtering was applied. Deposition was implemented with the aid of a pure B target (99.95 % purity, Mateck) under the Ar plasma condition (RF, 140 W). The sample holder was arranged to rotate to ensure uniform deposition of B films. The B deposition experiment was carried out two times under the identical working conditions, resulting in two B layers with thickness about 130 nm and 260 nm on W substrates, respectively, as shown in Fig. 1. Both smooth glass sheet and W substrate were coated with a B-films simultaneously using magnetron sputtering. The glass sheet was partially covered with adhesive tape during the coating process. After sputtering, the tape was removed, and the thickness of the deposited B-film was measured using a contact profilometer (Dektak 6 M, Bruker). Additionally, the thickness of each boron layer was analyzed using Focused Ion Beam combined with Scanning Electron Microscopy (FIB-SEM), and the results are presented in Fig. 12(b) and (c). The surface roughness (Ra) of the B-layer-1 and B-layer-2 is about 4.58 nm and 7.07 nm, respectively.

2.2. LIBS setup

Fig. 2 shows the schematic diagram of the LIBS experimental setup. A picosecond laser (EKSPLA, PL2241) operated in the third harmonic frequency (355 nm) of Nd:YAG with a pulse duration of 35 ps was employed as an ablation source. After being collimated by two apertures, the laser beam was focused vertically on the sample surface by a convex quartz lens (focal length-500 mm, diameter-50 mm). The sample was always placed in front of the focus point of the laser beam. The laser energy was fixed at 18 mJ before reaching the sample. The samples were ablated by laser in a vacuum chamber which was pumped down to 3×10^{-7} mbar to simulate the fusion device environment between reactor plasma discharges. Synchronously, the photons of the laser-induced plasma radiation were collected almost coaxial with an angle of ± 15° in the normal direction of the sample surface and then focused by two collection lens system, respectively. The plasma image, which was reduced 4.5 times by the collection lens, was coupled to the optical fiber #1 with a single-core diameter of 1.5 mm, and then imaged on the entrance slit of a custom-made spectrometer in Littrow-arrangement spectrometer (F-number: 4.3) equipped with an ICCD camera (iStar DH334T-18F, Andor). This spectrometer has a large etendue resulting in high detection sensitivity, but can only cover at once a selectable spectral range of 13 nm. Here, the spectral range was fixed from 695 nm-708 nm for the temporal evolution and depth analysis of B and W in this work. Moreover, the plasma image, which was reduced by a factor of 5 by the concave mirror, was coupled to a second optical fiber #2 with a single-core diameter of 0.6 mm. The advantage of concave mirrors is that there is no chromatic aberration by reflection. Consequently, compared to focusing lenses, concave mirrors are more suitable for detection and analysis across a wide spectral range (greater than tens to hundreds of nanometers). The other head of fiber #2 was selected to connect with two additional spectrometers. A Czerny-Turner compact spectrometer (AvaSpec-ULS2048CL-EVO, Avantes) was used to measure H and O elements over a large spectral range (350–900 nm) with moderate spectral resolution. An Echelle spectrometer in cross-dispersion arrangement (ESA4000 PLUS, LLA) was used to measure the temporal evolution of multiple B spectral lines in the UV–VIS regions (220–700 nm) with excellent spectral resolution ($\Delta\lambda = 0.02$ nm at $\lambda = 656$ nm) employing an imaged intensified camera (Kodak KAF-1001, LLA). However, the spectral sensitivity is due to the low f-number limited. The ESA Echelle spectrometer was only used to measure the temporal evolution of B I-249.68&249.77 nm, B II-412.19 nm and B II-494.04 nm of pure B sample, corresponding to Fig. 3(b). Beyond that, fiber #2 is always connected to the Avantes spectrometer. The Littrow-arrangement spectrometer could collect plasma from a region with a diameter of approximately 6.75 mm, while the Avantes and ESA Echelle spectrometers collected plasma from a region with a diameter of about 3 mm. The resulting spectrum represents the line integral of the plasma along the approximate Z-axis (laser incidence direction). Two multi-notch filters (355,532,1064 nm) were placed in front of fiber #1 and #2, which are used to block the scattered light from the laser and to protect the ICCD detector. This indicates that each of the three spectrometers was equipped with a multi-notch filter when in operation. A digital delay generator (DG645, Stanford R.S.) was used to achieve the synchronization of the ps-laser and the gate delay of three detectors. The applied gate delays and gate widths are described in detail in section 3.1. The samples were installed on a 2-D motoring translation stage for the sample movement to a new position with a precision of 0.01 mm. Finally, the variation in laser spot size was controlled by adjusting the distance between the laser- focusing lens and the target. The laser focal point is always behind the target surface. The corresponding

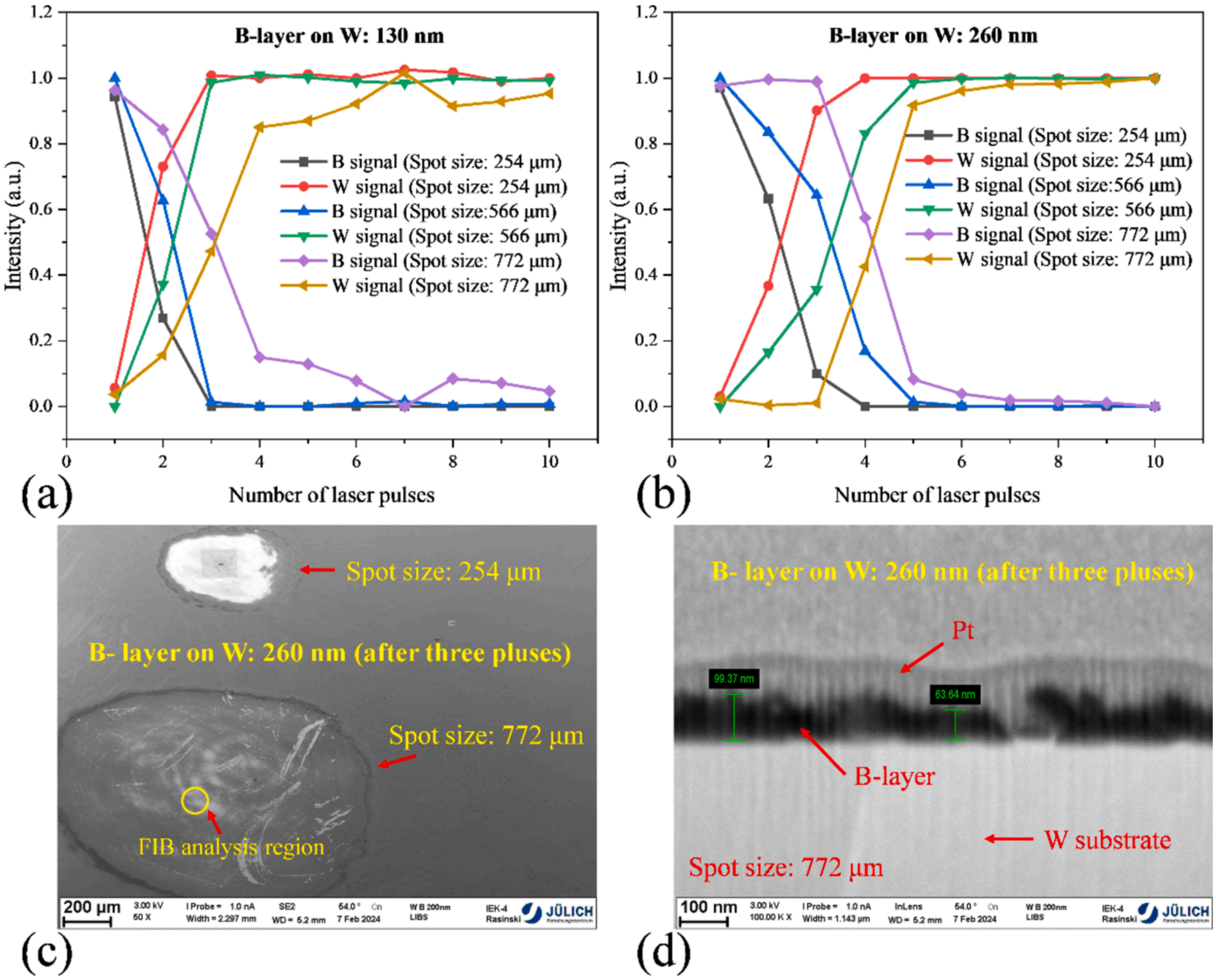

Fig. 9. Comparison of the normalized depth profiles for the B and the W signal for (a) the thin B-layer (about 130 nm) and (b) the thick B-layer (about 260 nm) on the W substrate with three spot size diameters studied. (c) The SEM image of laser spot sizes (after three pluses) at the 254 μm and 772 μm for the B layer (about 260 nm) on the W substrate. (d) The cross-section image of the yellow circle region obtained by FIB-SEM.

relationship between laser spot sizes and laser fluence is shown in Table 1.

3. Results and discussion

3.1. Characteristic lines and temporal evolution of B and W in a vacuum

Fig. 3(a) presents the typical B emission spectrum in the visible spectral region at the first laser shot with a spot size of 566 μm and a laser fluence of 7.2 J/cm^2 of the B-layer deposited on the W substrate. The lowering of the spectrum in the middle of the detection range is caused by a multi-notch filter. B II-412.2 nm and B II-703.2 nm are two “strong lines” have been identified to be in general suitable for the in-depth analysis at small collection solid angles in fusion devices. The corresponding energy level transition of these lines have a relatively large transition probability and a longer lifetime in a vacuum, as shown in Table 2. In addition, the B I transitions at 249.7 nm and 249.8 nm have also a signal strength in vacuum and are suitable for analysis, but are located in the ultraviolet region, thus more challenging for the detection set-up. For the *in-situ* and real-time element diagnosis of PFCs surface, the spectral range of LIBS in the visible region is easy to achieve due to the limitations of optical elements and windows. Moreover, the “strong lines” of the hydrogen isotopes D I-656.1 nm, and T I-656.0 nm which represent the reactor fuel species, the fusion ash He I-587.6 nm, and other favorable intrinsic impurity element-lines such as W I-429.5 nm, Mo I-550.6 nm from PFCs are also located in the visible region [36]. However, under LIBS plasma conditions, many other elements with strong and dense interference lines near 412.2 nm, such as W I-412.1, 412.2, 412.3 nm, and Mo I-412.1 nm [37]. Therefore, here the intensity and depth distribution of B II-703.2 nm and W I-698.4 and 699.3 nm lines were selected and investigated by the Littrow spectrometer equipped with the ICCD camera.

The temporal evolutions of intensities of B and W spectral lines were studied systematically by the pure B and pure W samples with laser spot size of 566 μm (7.2 J/cm^2) in order to obtain the optimal acquisition parameters, as shown in Fig. 3(b). The gate delay was set to $a \times 30$ ns and the gate width was fixed at 2 μs, where a is the measured step. This is also a reliable method to present temporal evolution information when the gate width is too short to get enough signal for the investigated spectral lines [38]. The radiation lifetime of the spectral characteristic line is related to many factors such as upper energy level E_k, transition probability A_{ki}, and plasma parameters (T_e and n_e). The lifetime of B II lines is significantly shorter than that of B I lines. It is understandable that with the rapid decrease of T_e and n_e after laser ablation in a vacuum, the higher the E_k, the shorter the lifetime of the spectral lines, as shown in Table 2. The results present that the lifetime of the high-energy level transition of B II lines is only 200 ns while the low-energy level transition of W I lines exceed 800 ns. Based on this, the optimal acquisition parameters of gate delay and gate width were set to 30 ns and 1 μs in this work, respectively.

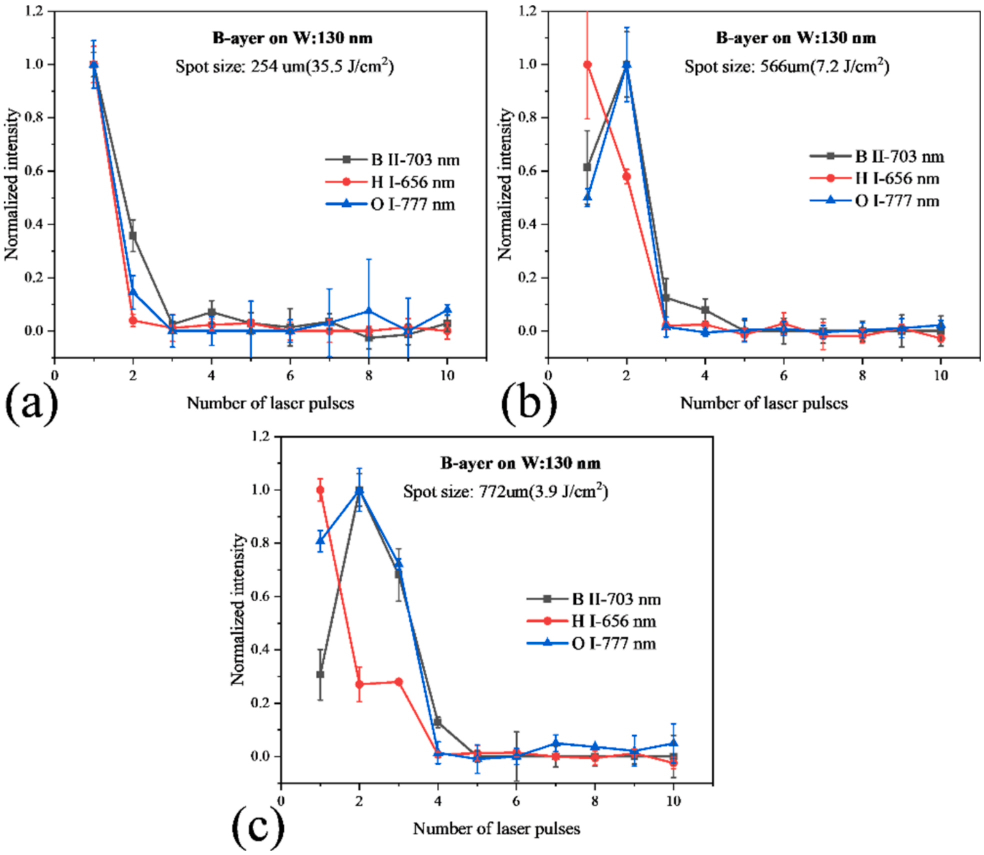

Fig. 10. Comparison of the normalized depth profiles for the B, O, H for the B-layer (about 130 nm) on W sample with spot size of (a) 254 μm (35.5 J/cm^2), (b) 566 μm (7.2 J/cm^2), and (c) 772 μm (3.9 J/cm^2), respectively.

3.2. Depth distribution characteristics of spectrum under different spot sizes (laser fluence)

The depth distributions of two different thicknesses of B-layer were characterized subsequently after determining the optimal spectral acquisition parameters. Fig. 4 (a) and (b) display the variation of LIBS spectra of the different B-layer thicknesses obtained by different laser pulses at spot size of 566 μm (7.2 J/cm^2). LIBS detects the distinct B signal in the first few laser pulses. For the thin B-layer sample (130 nm), the spectrum presents the W-substrate signal at the second laser pulse. While for a thick B-layer (260 nm), it requires three laser pulses to obtain the W signal. When the laser spot is adjusted to a larger size of 1297 μm (1.4 J/cm^2), distinctly different depth distributions appear as shown in Fig. 4 (c) and (d). It takes three laser pulses to detect the first W signal for the thin B layer sample and five laser pulses for the thick B layer. Apparently, the larger the spot sizes, the greater the number of laser pulses required to obtain the W-substrate signal. However, it is surprising that no clear B signal is detected at such a large spot size. On the contrary, the W-substrate signal is significantly enhanced compared with the small spot size. These results indicate that the variation trend of B and W lines intensity is diverse under the different laser spot sizes. Moreover, there are several weak W I signal near the wavelength of 703 nm at the 5th to 6th laser pulse of large spot size, which is not conducive to the depth analysis of B.

Hence, extraction of net B signal is an important step in its in-depth analysis [32]. The typical overlapping regions of spectral lines are shown in Fig. 5. In the spectrum of 4th laser pulse, the W signal has appeared and the intensity of the line overlap region is obviously greater than that of the 5th laser pulse. This means that the 4th laser pulse ablates part of the B and part of the W simultaneously. The extraction of net B signal is obtained by using the formula expressed as Eq. (1)[32].

$$S_{B\text{-}net}\ signal = S_{overlap\ region} - k \times S_{substrate} \tag{1}$$

where $S_{overlap\ region}$ is the integral intensity of the lines overlap region, $S_{substrate}$ is the sum of the integrated strengths of W I-698.4 and 699.3 nm. k is calculated by the ratio of $S_{overlap\ region}$ to $S_{substrate}$ in the pure W spectrum. This method is also suitable for the extraction of net D I-656.1 nm signal on W-substrate. Through the correction, the signal intensity of B reduces to 0 after B layer is completely ablated.

3.3. Spectral signal quality and depth resolution of B layer on W-substrates under different spot size (laser fluence)

Fig. 6 (a) presents the integrated depth profile of the B-layer (260 nm) on the W sample after 100 consecutive laser pulses with three different spot sizes. The 100 laser pulses were selected to more intuitively present the ablative crater profiles at different laser spot sizes. The laser fluence and average depth ablation rate corresponding to the different spot sizes are shown in Fig. 6 (b). The profile of the ablation craters indicate that the energy distribution of the laser beam is not a pure flat-top beam. As the spot sizes increase and the laser fluence decreases, there is a noticeable decrease in the depth ablation rate of the sample by the laser [40]. This confirms the results that more laser pulses are required to obtain the W-substrate signal at large spot sizes. The variation trend of B and W lines intensity under the different laser spot sizes are illustrated in Fig. 6 (c). The B signal intensity is the sum of the net B signal at first 10 laser pulses and the W signal intensity (W I-698.4 and 699.3 nm) is the sum of the 11th to 20th pulses. The maximum values of signal intensity of the two elements correspond to the different spot sizes and laser fluence, respectively. At local thermodynamic equilibrium (LTE), the optical emission intensity I_{ki} of a certain

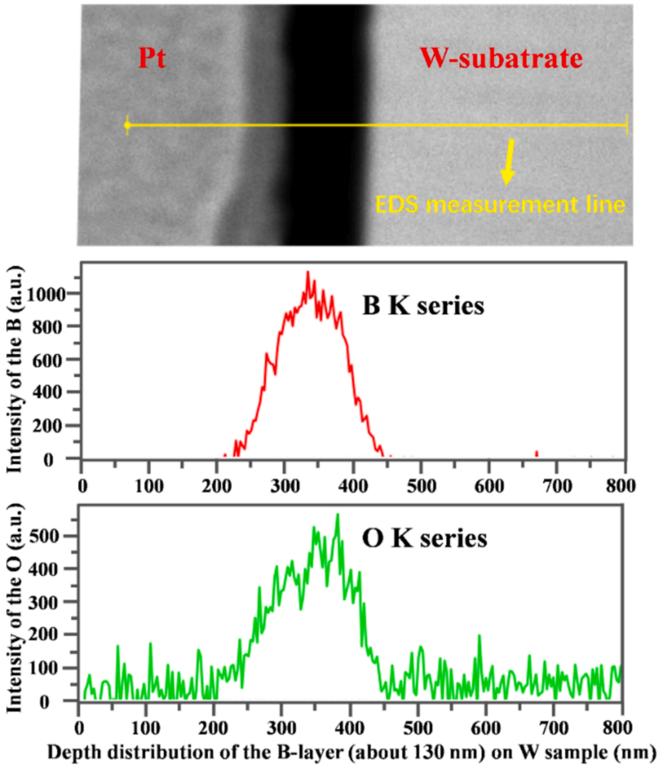

Fig. 11. Comparison of the depth profiles for the B, O for the B-layer (about 130 nm) on W sample measured by EDS. The first 0–230 nm is a layer of platinum plated during the EDS measurement. The measured intensity values of B and O represent only the relative evolution of element content with the depth profile.

transition λ_{ki} from the upper state E_k to the lower state E_i can be described in Eq. (2) [41].

$$I_{ki} = A_{ki} \bullet \frac{hc}{\lambda_{ki}} \bullet \frac{g_k}{U(T)} \bullet n \bullet e^{-E_k/k_B T} \tag{2}$$

where, the transition probability A_{ki}, wavelength of spectral line λ_{ki}, statistical weight of the upper level g_k, Boltzmann constant k_B and upper state E_k are all constants for a specific transition. *U(T)* is the partition function of the species related to *T*. Therefore, the intensity I_{ki} of the spectral line depends on the total density of particles *n* (positively correlated with the ablation mass) and the plasma temperature *T*. The variation of laser spot sizes will not only change the laser fluence, but also change the laser ablation area. Although a small spot size corresponds to a large laser fluence, too small spot size will cause a sharp decrease in the ablation mass, resulting in a reduction of the spectral intensity I_{ki}. While the spot sizes are too large, the decreased laser fluence is insufficient for effective ablation, which also leads to the reduction of I_{ki}. This may be the primary reason why the intensity of the element increases initially and then decreases with the enlargement of the spot size [42]. Furthermore, the plasma temperature *T* usually increases with the increase of the laser fluence, especially under the action of ps-laser which can effectively reduce the plasma shielding effect. The upper state E_k of B II-703.2 nm is much higher than that of W I-698.4 and 699.3 nm, as shown in Table 2. This makes the spot sizes corresponding to the optimal B signal significantly smaller than the optimal W signal.

The signal to noise ratio (S/N) and the signal to background ratio (S/B) are also evaluated for the B-layer analysis on W sample in fusion devices, as presented in Fig. 7. The signal value is the net intensity of the selected B II-703.2 nm and W I-699.3 nm lines. The noise value is calculated by the standard deviation of the continuum background in about 1 nm region of the spectrum (704.1 nm-705.1 nm). The background value is obtained by the continuum radiation at 704.8 nm. The S/N and S/B of the two elements also exhibit a trend of initially increasing and then decreasing with the spot size. The best S/N and S/B for B appear at the spot size between 400–650 μm (5–12 J/cm^2), while the best S/N and S/B for W appear at the spot size between 1000–1300 μm (1–3 J/cm^2). The results indicate that although excellent depth resolution and optimal W signal can be obtained at large spot sizes, the signal quality of B is a prerequisite for boronization analysis.

Fig. 8 shows the comparison of the depth distribution of B and W signal for the thicker B-layer (about 260 nm) on the W substrate for three different spot sizes. The intensity and depth profiles of elements change obviously with the increase of spot sizes. This is consistent with the variation trend of intensity shown in Fig. 6 (c). The increase of spot size makes the laser ablation to the interface of B layer and W-substrate require more pulses. In the case of a small spot size of 254 μm, it can be inferred that the pulse number of laser ablation to the interface is between 1–3 according to the change of depth profile. While for a large spot size of 772 μm, the number of laser pulses required is inferred to lay between 3–6. The results can only prove that the depth resolution can be improved under large beam spots, but the accurate interface and corresponding film thickness is difficult to be determined.

3.4. *The determination of the thickness of B layer on the W substrate*

Normalized intensity method and linear correlation method are powerful methods used in interface analysis by LIBS [43,44]. The linear correlation method is to obtain the linear correlation coefficient by measuring the interrelation between the spectral characteristic variables, and then determine the interface. However, the spectral difference between the film-element and the substrate-element is an important factor affecting the accuracy of this method. The existence of lines overlap region makes the method unsuitable for this work. The normalized intensity method is calculated using the following Eq. (3).

$$I_{film} = \frac{I'_{film}}{I'_{film} + I'_{substrate}}, I_{substrate} = \frac{I'_{substrate}}{I'_{film} + I'_{substrate}} \tag{3}$$

where I'_{film} is the normalized intensity of film-element, $I'_{substrate}$ is the normalized intensity of substrate-element. In this method, the interface is determined by the proportion of elements under the premise of stoichiometric ablation. The normalized intensity of $I_{film} = I_{substrate} = 0.5$ corresponds to the interface between B layer and the W substrate, as shown in Fig. 9(a) and (b). The intersection points of B signal and W signal under the same spot size is considered to be the number of pulses required for laser ablation to the interface. Compared with thin B layer, it is reasonable to require more pulses to reach the interface between thick B layer and W-substrate with the same spot size. The number of laser pulses corresponding to the interface of the two samples at different spot sizes is listed in Table 3. Simultaneously, the average ablation rate (*AAR*) of B layer is obtained by the following Eq. (4) [43].

$$AAR = \frac{T}{N_{0.5}} \tag{4}$$

where T is the thickness of B layer measured by profilometry and $N_{0.5}$ is the number of laser pulses corresponding to the interface. Fig. 9 (c) shows the comparison of SEM images under two different spot sizes in order to verify the accuracy of the results. After three laser pulses, the distinct features appeared on the surface of the two ablation craters for the B-layer (about 260 nm) on W sample. The small ablation crater has lost B and revealed the silver W-substrate while the brown B-layer still exists in the large ablation crater. The cross-section of the at the yellow circle region obtained by FIB-SEM are present in Fig. 9 (d). There is still a B layer in the thickness range of 64–99 nm in this region. The fluctuation of the thickness is due to the distribution of laser beam energy and the roughness of the film itself. Apparently, the results of the normalized intensity method are consistent with FIB-SEM, and the measurement error is acceptable for thick films.

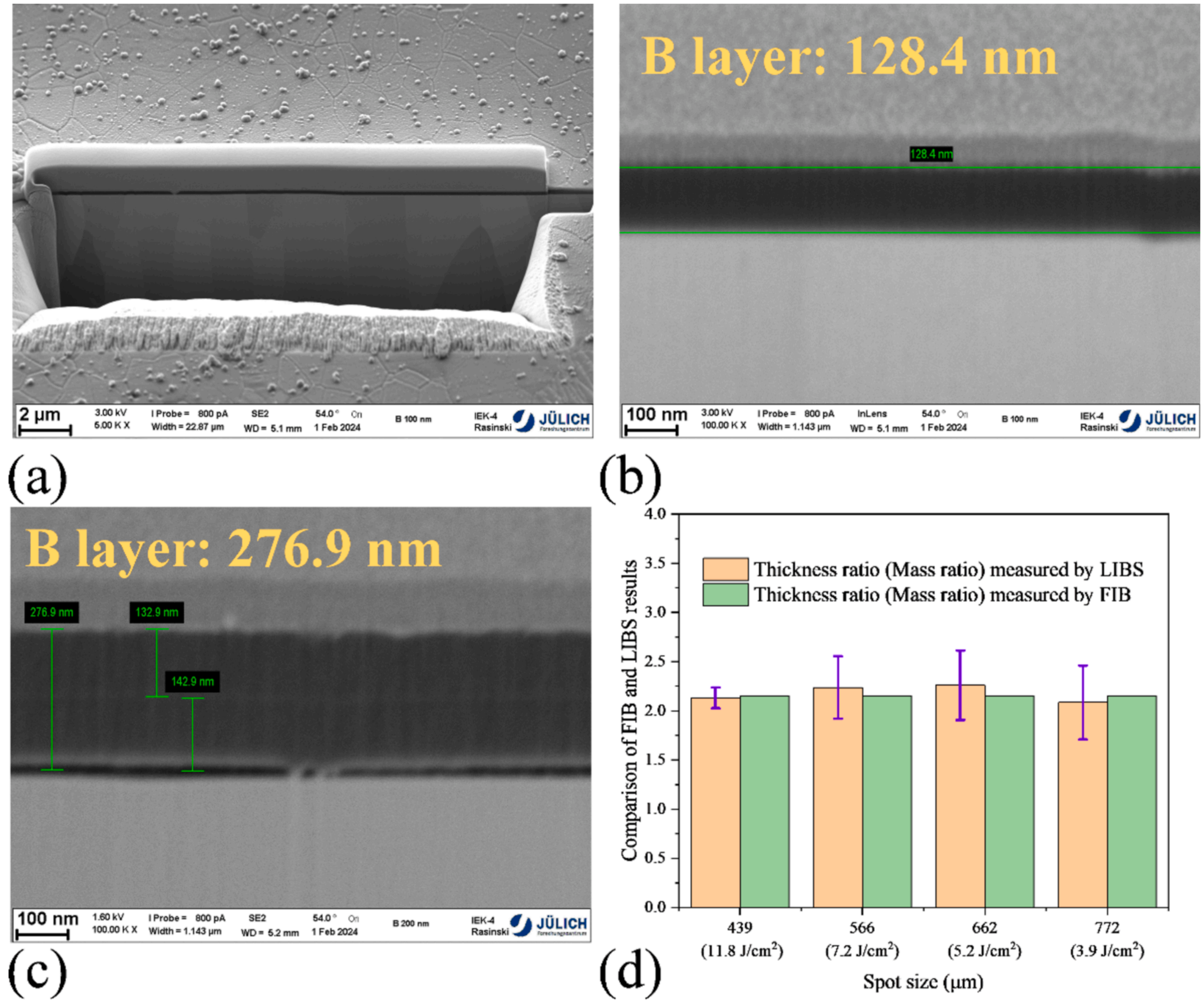

Fig. 12. (a) The schematic diagram of the B-layer on W sample at the typical locations which are analyzed by FIB-SEM. (b) The measurement results of single B layer thickness by FIB-SEM. (c) The measurement results of double B layer thickness by FIB-SEM. (d) The comparison of thickness ratio (mass ratio) results measured by LIBS and FIB-SEM.

Moreover, It is interesting that the number of laser pulses required for the thick B layer (about 260 nm) in Table 3 is not twice that of the thin film layer (about 130 nm), which results in the different average ablation rates. The reason is that the ablation rate of the laser for each pulse of the sample is varied, especially for the first several pulses [45]. The change of reflectance of the sample is the main possible reason for the difference of ablation rate in this work. The first laser pulse has the lowest ablation rate due to the mirror-like smooth surface of the sample before ablation. While with the increase of pulse number, a rough ablation crater with curved surface is formed, and the reflectivity gradually decreases to a relatively stable value.

In addition to the change of reflectivity, the influence of the water layer absorbed on the sample surface could not be ignored. The samples are inevitably exposed to air when moving from the magnetron sputtering device to the LIBS chamber. The water layer on the sample surface should come from the adsorption of H_2O in the atmosphere. Therefore, the B signal obtained by the first pulse of LIBS is often weaker than the second pulse at large fluence, as shown in Fig. 8. To confirm this phenomenon, the normalized depth distribution profiles of H, O, and B signals are further investigated and presented in Fig. 10. The maximum value of the H signal appears at the first laser pulse regardless of the spot sizes. The constant presence of oxygen at the first pulse is also favorable evidence for the presence of water layer absorbed on the sample surface. It is interesting that the O signals change in a similar trend as B except for the first laser pulse. This is reasonable to infer that the O signal of first laser pulse should be mainly contributed by the water layer, while the subsequent laser pulses should be mainly contributed by the boron oxide. This is also confirmed by Energy Dispersive X-ray Spectroscopy (EDS) results as shown in Fig. 11. Apart from the initial surface, the depth profiles of B and O are almost identical. Although the profile of H cannot be obtained by EDS, the fact that the depth profile of O is wider than B on the sample surface also indicates the presence of a water layer. In addition, more analytical methods such as Thermal Desorption Spectroscopy (TDS) and X-ray Photoelectron Spectroscopy (XPS) are needed to understand the formation mechanism of water layer and boron oxide in the future. The reflectance and water layer make it difficult to calculate thickness only by normalized intensity method. Moreover, this method neglects the physical properties of the material itself, the laser ablation rate on different materials, the roughness of the sample and the energy distribution of the laser beam [46]. It is necessary

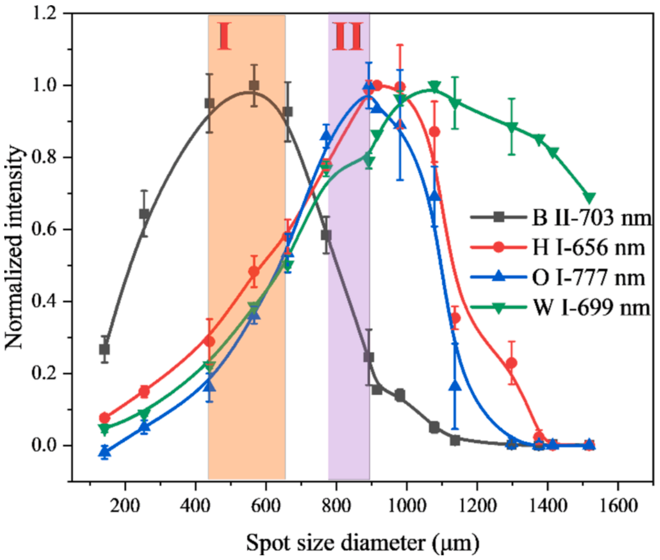

Fig. 13. The variation trend of normalized spectral intensity of B, H, O, W with spot size diameters. The region I represents the spot size most suitable for obtaining the optimal B signal intensity and the II represents the spot size for obtaining the optimal depth resolution.

to establish a reasonable physical model to gradually resolve these influencing factors and attempt to get accurate thickness information.

As is described above, another intensity ratio method based on Eq. (2) is proposed to evaluate the thickness of B layer, as shown in Eq. (5).

$$R_{t21} = \frac{I_{b2}/I_{w2}}{I_{b1}/I_{w1}} \tag{5}$$

where R_{t21} is the thickness ratio of layer 2 to layer 1. I_b and I_w are the sum of the intensity of layer elements such as B and substrate elements such as W, respectively. In this work, the B signal intensity is the sum of all laser pulses and the W signal intensity is the sum of the 11th to 20th pulses (Only W-substrate exists and no B). It relies on the proportional relationship between element intensity I_{ki} and content n to obtain the thickness information under consistent experimental conditions. Fig. 12 (b) and (c) show the measured values of thin B-layer and thick B-layer sample respectively, which are consistent with the results of the profiler meter. The thickness ratio measured by FIB is about 2.15. The comparison of thickness ratio (mass ratio) results of LIBS measurements and FIB-SEM evaluation are presented in Fig. 12 (d). The preparation process and the material composition of the two samples with different B-layer thicknesses are consistent. Under the same laser spot size, the thickness of the boron layer determines the amount of laser ablation, and thus determines the spectral intensity. Under the premise of the same density of B layer, the thickness ratio could be regarded as equal to the mass ratio. The calculated values of LIBS agree well with those of FIB-SEM under four typical fluence. This is reasonable because the variation range of laser fluence is located in the linear ablation region of ps-LIBS. The prerequisite for this method is the availability of a standard sample of known thickness. For example, the spectral information of the standard sample is obtained before the *in-situ* diagnosis of the boron layer thickness, and then the spectral information of the unknown thickness of the B layer is measured under completely consistent experimental conditions, and finally the thickness ratio is obtained. The applicability of this method will be further verified under B-layer samples with different thicknesses in the future works.

3.5. *The optimal scheme for B layer measurement*

After plasma discharge, the wall surface of the fusion device will exhibit mixed composition layers of multiple materials due to the material erosion/deposition cycle. The B will be redistributed in the vessel. It is significant to understand the PWI behavior such as fuel retention (D/T), material erosion and impurity redeposition (such as O/W, etc.) after the boronization. For this purpose, the variation trend of normalized spectral intensity of B, H, O, W under the different spot sizes were studied systematically, as depicted in Fig. 13. The normalized intensity of B, H and O is calculated by the sum of first 10 laser pulses and the normalized intensity of W is the sum of the 11th to 20th pulses. The maximum spectral line intensity of each element corresponds to the different spot sizes, which is mainly related to the spectroscopic parameters shown in Table 2. The optimal laser characteristic conditions should be selected according to different investigated objectives. The region I covers spot sizes in the 450–650 μm range (corresponding to laser fluence of 5–11 J/cm^2), which represents the spot size most suitable for obtaining the optimal B signal intensity. This region can be dedicated to the lifetime measurement of B films because it has the best detection limit. While the region II covers spot sizes in the 750–850 μm range (2.5–3.2 J/cm^2), which is the prime candidate for determining the homogeneity of thin boron film. Under this condition, not only the depth resolution is improved, but also the satisfactory fuel and impurity signals can be obtained.

4. Conclusion

In this work, the signal intensity and depth measurement of B-films with two different thicknesses on W-substrate have been systematically investigated by ps-LIBS in a vacuum. A gate delay of 30 ns and gate width of 1 μs were identified as the optimal spectral acquisition parameters for *in-situ* measurements of B-layer on W wall. The B II-703.2 nm lines and its adjacent W I lines are suitable for detection in the visible spectral region. Both the characteristic spectrum and the profile of the ablation crater of ps-LIBS present that the average laser ablation rate decreases with the increase of spot size. However, the excessive spot size may cause the laser fluence to fall below the excitation threshold of the B signal, which is not acceptable for LIBS analysis. Influenced by the spectroscopic parameters, plasma parameters and ablation mass, the maximum values of signal intensity of the B and W elements correspond to the different spot sizes and laser fluence, respectively. The interface between B-layers and W-substrate was determined and the average ablation rate of ps-LIBS on B films was estimated by normalized intensity method. The LIBS results show that the laser ablation rate of boron layer changes continuously in the first few pulses due to the influence of surface reflectivity, absorbed water layer, laser beam profile, sample roughness and so on. A complex physical model is required for normalized intensity method to invert the thickness information through the interface, which will be carried out in the subsequent work. The intensity ratio method was developed to calculate the thickness ratio of boron layers, which can be used as a candidate for thickness analysis, especially for thin layers. The calculated values of LIBS agree well with those of FIB-SEM. Moreover, the optimal laser characteristic parameters for *in-situ* B measurement by ps-LIBS were obtained. The region I covers spot sizes in the 450–650 μm range (corresponding to laser fluence of 5–11 J/cm^2), which is suitable for obtaining the optimal B signal intensity. While the region II covers spot sizes in the 750–850 μm range (2.5–3.2 J/cm^2), which is the prime candidate for determining the homogeneity of boron film. In addition, it should be noted that after boronization and plasma discharge, the first wall surface is usually a B-mixed layer. The ablative rates and spectral characteristics of laser-induced B-mixed layer plasma need further verification. How to determine the thickness of the mixed layer and the content of B still needs further investigation. The above results would provide valuable information about the thickness analysis of boron films using the real-time and *in-situ* LIBS system in fusion devices.

CRediT authorship contribution statement

Huace Wu: Writing – original draft, Methodology, Investigation, Formal analysis, Conceptualization. **Rongxing Yi:** Validation, Formal analysis. **Anne Houben:** Resources, Investigation. **Sebastijan**

Brezinsek: Writing – review & editing, Project administration, Methodology, Funding acquisition. **Marcin Rasinski:** Visualization, Validation. **Cong Li:** Investigation. **Gennady Sergienko:** Software. **Yunfeng Liang:** Visualization. **Timo Dittmar:** Visualization. **Hongbin Ding:** Writing – review & editing, Supervision, Project administration, Conceptualization.

Declaration of competing interest

The authors declare that they have no known competing financial interests or personal relationships that could have appeared to influence the work reported in this paper.

Acknowledgements

This research was supported by National Key R&D Program of China (No. 2023YFF0714901), the National MCF Energy Research and Development Program of China (Nos. 2022YFE03200100, 2022YFE03200200, 2019YFE03080100), the National Natural Science Foundation of China (Nos.12375208,12005034) and the China Scholarship Council. This work has been carried out within the framework of the EUROfusion Consortium, funded by the European Union via the Euratom Research and Training Programme (Grant Agreement No 101052200 - EUROfusion). Views and opinions expressed are however those of the author(s) only and do not necessarily reflect those of the European Union or the European Commission. Neither the European Union nor the European Commission can be held responsible for them.

Data availability

Data will be made available on request.

References

[1] J. Li, M. Shimada, Y. Zhao, et al., Wall conditioning towards the utilization in ITER, J. Nucl. Mater. 415 (2011) S35–S41.

[2] T. Nakano, S. Higashijima, H. Kubo, et al., Boronization effects using deuterated-decaborane ($B_{10}D_{14}$) in JT-60U, J. Nucl. Mater. 313 (2003) 149–152.

[3] C.H. Skinner, F. Bedoya, F. Scotti, et al., Advances in boronization on NSTX-Upgrade, Nucl. Mater. Energy 12 (2017) 744–748.

[4] C. Martin, M. Diez, A. Campos, et al., First post-mortem analysis of deposits collected on ITER-like components in WEST after the C3 and C4 campaigns, Phys. Scr. 96 (2021) 124035.

[5] J. Winter, Wall conditioning in fusion devices and its influence on plasma performance, Plasma Phys. Control. Fusion 38 (1996) 1503–1542.

[6] C.P. Dhard, S. Brezinsek, M. Mayer, et al., Plasma-wall interaction studies in W7-X: main results from the recent divertor operations, Phys. Scr. 96 (2021) 124059.

[7] H.Y. Wang, X.M. Wang, J.H. Wu, et al., Boronization during the First Plasma Operation on EAST, in, Iop Publishing Ltd, Stockholm, SWEDEN, 2007.

[8] S.H. Hong, K.S. Lee, K.P. Kim, et al., First boronization in KSTAR: Experiences on carborane, J. Nucl. Mater. 415 (2011) S1050–S1053.

[9] S. Sereda, S. Brezinsek, E. Wang, et al., Impact of boronizations on impurity sources and performance in Wendelstein 7-X, Nucl. Fusion 60 (2020) 086007.

[10] M. Dibon, V. Rohde, F. Stelzer, et al., New boronization system at ASDEX Upgrade, Fusion Eng. Des. 165 (2021) 112233.

[11] G. Bodner, A. Gallo, A. Diallo, et al., Initial results from boron powder injection experiments in WEST lower single null L-mode plasmas, Nucl. Fusion 62 (2022) 086020.

[12] O.I. Buzhinskij, Y.M. Semenets, Review of in situ boronization in contemporary tokamaks, Fusion Technol. 32 (1997) 1–13.

[13] J. Yang, S.H. Hong, D. Kim, et al., Effect of boronization in VEST: Achieving 0.1 MA discharge, Fusion Eng. Des. 137 (2018) 358–361.

[14] R. Lunsford, V. Rohde, A. Bortolon, et al., Active conditioning of ASDEX Upgrade tungsten plasma-facing components and discharge enhancement through boron and boron nitride particulate injection, Nucl. Fusion 59 (2019) 126034.

[15] F. Nespoli, N. Ashikawa, E.P. Gilson, et al., First impurity powder injection experiments in LHD, Nucl. Mater. Energy 25 (2020) 100842.

[16] M. Mayer, M. Balden, S. Brezinsek, et al., Carbon erosion/deposition on the divertor of W7-X during the operational period OP 1.2b, Nucl. Fusion 62 (2022) 126049.

[17] Z. Wang, T.B. Yuan, Z.Y. Hou, et al., Laser-induced breakdown spectroscopy in China, Front. Phys. 9 (2014) 419–438.

[18] H.C. Wu, C. Li, D. Wu, et al., Characterization of laser-induced breakdown spectroscopy on tungsten at variable ablation angles using a coaxial system in a vacuum, J. Anal. at. Spectrom. 36 (2021) 2074–2084.

[19] Z.H. Hu, H.C. Wu, X. Bai, et al., Characterization of impurity distribution and composition on the shutter plate for an optical diagnosis in EAST tokamak using laser-induced breakdown spectroscopy, Fusion Eng. Des. 197 (2023) 114078.

[20] C. Li, C.L. Feng, H.Y. Oderji, et al., Review of LIBS application in nuclear fusion technology, Front. Phys. 11 (2016) 114214.

[21] G.S. Maurya, A. Marín-Roldán, P. Veis, et al., A review of the LIBS analysis for the plasma-facing components diagnostics, J. Nucl. Mater. 541 (2020) 152417.

[22] P. Veis, S. Atikkuke, A.M. Roldan, et al., LIBS analysis of samples from the COMPASS vacuum chamber after liquid metal experiments - Li campaign, Nucl. Mater. Energy 25 (2020) 100809.

[23] J.M. Liu, D. Wu, D.Y. Zhao, et al., Ex-situ quantification of impurity deposition depth on HL-2A divertor graphite tile by laser-induced breakdown spectroscopy, Fusion Eng. Des. 195 (2023) 113930.

[24] S. Almaviva, L. Caneve, F. Colao, et al., LIBS measurements inside the FTU vacuum vessel by using a robotic arm, Fusion Eng. Des. 169 (2021) 112638.

[25] A. Huber, B. Schweer, V. Philipps, et al., Study of the feasibility of applying laser-induced breakdown spectroscopy for *in-situ* characterization of deposited layers in fusion devices, Phys. Scr. T145 (2011) 014028.

[26] J. Karhunen, A. Hakola, J. Likonen, et al., Applicability of LIBS for *in-situ* monitoring of deposition and retention on the ITER-like wall of JET - Comparison to SIMS, J. Nucl. Mater. 463 (2015) 931–935.

[27] D.Y. Zhao, C. Li, Z.H. Hu, et al., Remote *in-situ* laser-induced breakdown spectroscopic approach for diagnosis of the plasma facing components on experimental advanced superconducting tokamak, Rev. Sci. Instrum. 89 (2018) 073501.

[28] G. Maddaluno, S. Almaviva, L. Caneve, et al., Detection by LIBS of the deuterium retained in the FTU toroidal limiter, Nucl. Mater. Energy 18 (2019) 208–211.

[29] X. Jiang, G. Sergienko, B. Schweer, et al., Design and development of a LIBS system on linear plasma device PSI-2 for in situ real-time diagnostics of plasma-facing materials, Nucl. Mater. Energy 12 (2017) 1224–1230.

[30] P. Paris, I. Jogi, K. Piip, et al., In-situ LIBS and NRA deuterium retention study in porous W-O and compact W coatings loaded by Magnum-PSI, Fusion Eng. Des. 168 (2021) 112403.

[31] N. Gierse, B. Schweer, A. Huber, et al., In situ characterisation of hydrocarbon layers in TEXTOR by laser induced ablation and laser induced breakdown spectroscopy, J. Nucl. Mater. 415 (2011) S1195–S1198.

[32] L.Y. Sun, D. Wu, C. Li, et al., Characterization of the impurity features deposited on the boronization tungsten tiles exposed in KSTAR tokamak using laser-induced breakdown spectroscopy, Nucl. Mater. Energy 31 (2022) 101174.

[33] D. Zhao, S. Brezinsek, R. Yi, et al., Investigation of boron distribution and material migration on the W7-X divertor by picosecond LIBS, Phys. Scr. 97 (2022) 024005.

[34] D.Y. Zhao, D. Wu, J. Oelmann, et al., Highly depth-resolved characterization of fusion-related tungsten material based on picosecond laser-induced breakdown spectroscopy, J. Anal. at. Spectrom. 35 (2020) 2867–2879.

[35] S. Mittelmann, J. Oelmann, S. Brezinsek, et al., Laser-induced ablation of tantalum in a wide range of pulse durations, Appl. Phys. A-Mater. Sci. Process. 126 (2020) 672.

[36] C. Li, L.Y. Sun, Z.H. Hu, et al., An *in-situ* diagnostic method for monitoring of fuel retention on the first wall under long-pulse operation of experimental advanced superconducting tokamak, Phys. Scr. T171 (2020) 014069.

[37] M. Imran, Z.H. Hu, F. Ding, et al., Depth-resolved analysis of multi-element impurity deposition on test tiles in EAST tokamak by using laser-induced breakdown spectroscopy, Nucl. Mater. Energy 34 (2023) 101379.

[38] H.C. Wu, C. Li, D. Wu, et al., Spatiotemporal dynamic characterization of the laser-induced plasma of a mixed material (WCCu) under variable ablation angles in a vacuum, J. Anal. at. Spectrom. 37 (2022) 2069–2081.

[39] Standards and Technology (2023). https://dx.doi.org/10.18434/T4W30F.

[40] H.C. Wu, D. Wu, C. Li, et al., Effect of laser ablation angles on the ablated depth/mass and spectral intensity of laser-induced plasma on EAST-like plasma-facing materials in a vacuum, Spectroc. Acta Pt. B-Atom. Spectr. 202 (2023) 106647.

[41] D.W. Hahn, N. Omenetto, Laser-Induced Breakdown Spectroscopy (LIBS), Part I: Review of Basic Diagnostics and Plasma–Particle Interactions: Still-Challenging Issues Within the Analytical Plasma Community, Appl. Spectrosc. 64 (2010) 335A–A366.

[42] J.M. Liu, D. Wu, X.H. Hu, et al., Study of spectral intensity of the laser ablated tungsten plasma and ablation mass at various laser spot sizes and laser fluence in vacuum environment, Spectroc. Acta Pt. B-Atom. Spectr. 199 (2023) 106569.

[43] S.M. Aberkane, M. Abdelhamid, K. Yahiaoui, et al., Depth profiling of alumina thin films using laser induced breakdown spectroscopy: Structural and morphological dependence, Thin Solid Films 653 (2018) 293–300.

[44] C. Li, J. Oelmann, S. Brezinsek, et al., Quantitative analysis of elemental depth on Wendelstein 7-X divertor baffle screws by picosecond laser-induced breakdown spectroscopy, Spectroc. Acta Pt. B-Atom. Spectr. 160 (2019) 105689.

[45] D.Y. Zhao, N. Gierse, J. Wegner, et al., Ablation mass features in multi-pulses femtosecond laser ablate molybdenum target, Nucl. Instrum. Methods Phys. Res. Sect. B-Beam Interact. Mater. Atoms 418 (2018) 54–59.

[46] S.M. Liu, C. Li, H.C. Wu, et al., Experimental and model study of LIBS depth profile for multilayer deposition materials, Spectroc. Acta Pt. B-Atom. Spectr. 209 (2023) 106783.